A Three-Point Dixon Method for Water and Fat Separation Using 2D and 3D Gradient-Echo Techniques

Yi Wang, MS • Debiao Li, PhD • E. Mark Haacke, PhD • Jeffrey J. Brown, MD

A water and fat separation technique based on a three-point Dixon method using two-dimensional (2D) and three-dimensional (3D) gradient-echo sequences and a new phase-unwrapping approach is presented. Using velocity-compensated sequences, three images, with water and fat protons in phase, opposed phase, and in phase, were acquired in an interleaved fashion for each phase-encoding line of the image. A fast 2D scan permitted acquisition of images within a single breathhold, eliminating respiratory motion artifacts. The 3D sequence allowed coverage of a large region of interest with thin, contiguous slices. To correct field inhomogeneity effects, phase unwrapping was required. This was accomplished by comparing the corresponding pixels in the two water and fat in-phase images on a pixel-by-pixel basis. This phase-unwrapping approach is faster, more reliable, and requires less user interfacing than other methods. The water and fat separation method performed well in various parts of the body.

Index terms: MRI • Water and fat separation • Phase unwrapping • Image processing • Chemical shift

JMRI 1998; 8:703–710

Abbreviations: FOV = field of view, Gd-DTPA = gadolinium-diethylenetriamine pentaacetic acid, MPR = multiplanar reconstruction, RF = radiofrequency, 2D = two-dimensional, 3D = three-dimensional.

From the Mallinckrodt Institute of Radiology at Washington University Medical Center, 510 South Kingshighway Boulevard, St. Louis, MO 63110. Received January 14, 1997; revision requested June 16; revision received August 25; accepted September 12. Part of this study was presented at the third annual meeting of the Society of Magnetic Resonance, Nice, France, 1995. Y.W. was supported in part by NIH Grant DK49393. **Address reprint requests to** D.L.

WATER AND FAT ARE the two major contributors to signal in proton MRI of the human body. Accurate quantification of water and fat components has important applications in characterizing tumors of adrenal glands and may have additional utility in evaluating liver and bone marrow disease (1). Because of the short T1 of lipid protons, fatty tissue has a higher signal intensity than most water tissues in T1-weighted images and can often significantly reduce the visual contrast between tissues. Thus, elimination of fat signal can be very helpful in visualizing the optic nerve, breast tumors, bone marrow lesions, and liver, renal, and pancreatic pathology. Elimination of fat signal is also useful for confirming the presence of fat in tumors such as lipomas, angiomyolipomas, and myelolipomas and for reducing chemical shift and motion artifacts related to the presence of the strong fat signal (2).

Various methods (3–19) have been proposed to eliminate the fat signal or separate fat and water components in MRI, including selective saturation (3,4), inversion recovery (5,6), and two- and three-point Dixon methods (7–16). Among these, the selective saturation and the two-point complex Dixon methods suffer from magnetic field inhomogeneity effects. The inversion recovery method, which uses the differences in T1 between fat and water tissues, requires a long imaging time, especially for a spin-echo sequence. The two-point Dixon method (7) has been used commonly for water and fat separation because of its ease of implementation and potential high accuracy. It uses two images with the water and fat signals in phase in one image and opposed phase in the other, acquired by varying the TE. Separated water and fat images can be generated by adding and subtracting these images. However, in the presence of field inhomogeneities, tissue phases at the two TEs deviate from the expected values, and information from the water and fat images is mixed. Careful shimming can significantly improve global field homogeneity in most modern imaging systems. However, local variations in magnetic field, both from internal susceptibility and the applied static field, remain. To overcome this problem, magnitude images were used for addition and subtraction to generate water and fat images in the two-point Dixon method. However, the resulting images contain only dominant signal (addition) and nondominant signal (subtraction), respectively. Thus, each image can contain a combination of water and fat signals from pixel to pixel.

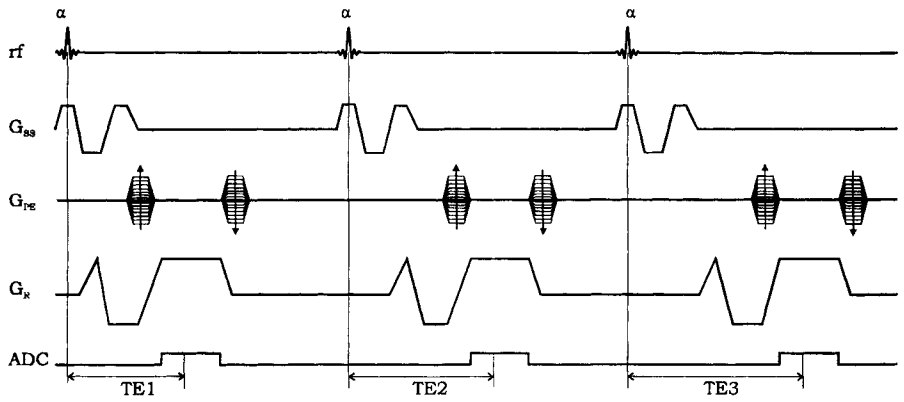

Figure 1. Diagram of a 2D gradient-echo, velocity-compensated, interleaved scan with three TEs corresponding to water and fat being in phase, opposed phase, and in phase. rf = radiofrequency pulse, G_{SS} = slice-select gradient, G_{PE} = phase-encoding gradient, G_R = readout gradient, ADC = analog-to-digital converter.

Many modifications (8–16) to Dixon's original method have been proposed with spin-echo sequences. Haacke et al (8) first proposed a three-point method to simultaneously separate water and fat and extract field inhomogeneity information. Glover and Schneider (9) used a similar approach with phase shifts of 0, $-\pi$, and π between water and fat to overcome the field inhomogeneity effects. They developed a two-step phase-unwrapping algorithm to solve the troublesome phase aliasing problem. Borrello et al (10) used a uniform phantom to obtain a field map, which was then used to correct the patient image. This approach works well only when any patient-induced field inhomogeneity is negligible. Hardy et al (11) proposed a T2-weighted fast spin-echo three-point Dixon technique based on the readout gradient shift instead of the more commonly used π pulse shift. Zhang et al (12) recently proposed a "sandwich" sequence that can be used to separate water and fat at .35 T. This method is difficult to implement at 1.5 T because of the small time difference between in-phase and opposed-phase TEs at the higher field strength. Spin-echo sequences were used in most of these studies. If the π pulse is shifted by τ relative to the 90° pulse, the resulting spin-echo image will have a field inhomogeneity-induced phase term determined by 2τ, the effective gradient echo time. Compared to gradient-echo sequences, the effective gradient-echo time in spin-echo sequences could be kept quite small. However, these sequences have a relatively long imaging time and thus have limited application in abdominal imaging because of respiratory motion artifacts. Finally, most previously proposed methods use two-dimensional (2D) data acquisition sequences.

The basis of all of these three-point Dixon methods is the collection of local field information with phase images. In each technique, phase unwrapping is required. Phase wrapping, or aliasing, occurs because the calculated phase has a dynamic range from $-\pi$ to π. Large field inhomogeneities may induce a phase greater than π. For example, in a 1.5-T system, a 1.675-ppm field shift will cause a phase shift of π when TE = 4.8 msec, which may result in phase aliasing and induce water and fat misclassification if not accounted for. The phase-unwrapping process produces the true phase from the calculated phase by detecting the presence of phase aliasing and then adding or subtracting a multiple of 2π from the calculated phase. Current phase-unwrapping methods, such as region growing (9,13) and line tracing (10,20), rely on voxel connectivity and field continuity. It is assumed that the phase in the adjacent pixels will not exceed a certain threshold, eg, π. However, this assumption may not be valid in practical imaging, especially in areas where field shimming may not work well, such as at air/tissue interfaces. Thus, if there is a significant field susceptibility variation, the phase change between the two adjacent pixels could exceed the preset threshold and phase unwrapping will fail. In addition, if there are tissues isolated by noise, a separate seed must be given to each tissue segment. This requires increased user interaction and is prone to operator error, because the seed points must be chosen as points free from aliasing. Finally, any error in phase unwrapping at one pixel will propagate throughout the rest of the image. Methods of overcoming these problems have been proposed (9,21); however, limitations still exist.

In this paper, we present a method that is able to phase unwrap the data locally based on individual in-phase pixel values. We apply it in conjunction with 2D and three-dimensional (3D) gradient-echo methods and demonstrate potential clinical applications of the water and fat separation process in the brain, abdomen, breast, and knee.

• MATERIALS AND METHODS

Data Acquisition Techniques

We have developed both 2D and 3D gradient-echo sequences to collect images with three different TEs (4.8 msec, 7.2 msec, and 9.6 msec), corresponding to fat and water being in-phase, opposed-phase, and in-phase at 1.5 T, respectively. To avoid potential motion effects and slice misregistration, each phase-encoding line was acquired interleaved before the phase-encoding gradient was incremented. The 2D sequence was fast enough that a scan could be completed within a single breath-hold thereby eliminating respiratory motion artifacts. The 3D sequence generated thin contiguous slices that could be easily postprocessed using multiplanar reconstruction (MPR) to view a region of interest from different orientations. Both sequences were velocity compensated in slice-select and readout directions to avoid ghosting artifacts secondary to pulsatile blood flow in major vessels. The 2D sequence structure is illustrated in Figure 1. The 3D sequence was similar, except that it had a partition-encoding table in the slice-select direction.

Phase Unwrapping

The chemical shift between water and fat is 3.35 ppm, leading to a 208-Hz frequency shift for a static magnetic field of 1.5 T. Assuming water and fat spectra are δ functions, the signals in tissue containing both water and fat components can be represented as follows:

$$I(t) = (\rho_w + \rho_f e^{i\delta\omega t}) e^{i\Delta\omega t + \varphi_0} \quad [1]$$

where ρ_w and ρ_f are the amplitude of the water and fat

Table 1
Phase Shifts of the Three Images

Echo time:	4.8 msec	7.2 msec	9.6 msec
Image phase:	φ_A	φ_B	φ_C
Water-dominated pixel:	$\varphi_0 + \varphi_1$	$\varphi_0 + \frac{3\varphi_1}{2}$	$\varphi_0 + 2\varphi_1$
Fat-dominated pixel:	$\varphi_0 + \varphi_1$	$\varphi_0 + \frac{3\varphi_1}{2} + \pi$	$\varphi_0 + 2\varphi_1$

Note.—φ_0 is a constant phase caused by RF penetration and eddy currents, which is present in all three images; and φ_1 is the phase shift caused by the local field inhomogeneity, which is a linear function of the TE.

Table 2
Phase Behavior of the Two Water and Fat In-Phase Images for the Detection of Phase Aliasing

		φ'_A		φ_C	
θ	Case	Calculated Phase	True Phase	Calculated Phase	True Phase
0	a	$[-\pi/2, \pi/2]$	$(-\pi/2, \pi/2)$	$(-\pi, \pi)$	$(-\pi, \pi)$
2π	b	$[\pi/2, \pi]$	$[\pi/2, \pi)$	$[-\pi, 0]$	$[\pi, 2\pi)$
-2π	c	$[-\pi, -\pi/2]$	$[-\pi, \pi/2]$	$[0, \pi]$	$[-2\pi, -\pi]$
-2π	d	$[-\pi, -\pi/2]$	$[\pi, 3\pi/2]$	$[0, \pi]$	$[2\pi, 3\pi]$
2π	e	$[\pi/2, \pi]$	$[-3\pi/2, -\pi)$	$[-\pi, 0]$	$[-3\pi, -2\pi)$
0	f	$[0, \pi/2]$	$(-3\pi/2, -2\pi)$	$[0, \pi]$	$(-3\pi, -4\pi)$
0	g	$[-\pi/2, 0]$	$(3\pi/2, 2\pi)$	$[-\pi, 0]$	$(3\pi, 4\pi)$

signals to be determined; $\Delta\omega$ is the offset frequency due to the local field inhomogeneity (ΔB_0), $\Delta\omega = \gamma \cdot \Delta B_0$, where γ is the gyromagnetic ratio of the proton; $\delta\omega$ is the frequency difference between water and fat due to chemical shift; φ_0 is a tissue-dependent phase shift caused by radiofrequency (RF) penetration and eddy currents independent of the TE. The time-dependent phase term, $\Delta\omega \cdot t$, can be rewritten as $\varphi_1 = \gamma \cdot \Delta B \cdot \mathrm{TE}$. Images are acquired with phase shifts of 0 (φ_A), π (φ_B), and 2π (φ_C) between water and fat caused by chemical shift. The corresponding phases for the three images at different TEs are given in Table 1.

To remove field inhomogeneity effects, φ_0 and φ_1 must be extracted from the phase images. First, the field-independent phase term, φ_0, is found from

$$\varphi_0 = 2 \cdot \varphi_A - \varphi_C \qquad [2]$$

It is reasonable to assume that φ_0 is less than π. If the calculated φ_0 is greater than π, it is assumed that φ_0 is aliased and it is then shifted back to $[-\pi, \pi]$ by adding or subtracting 2π. φ_0 is then removed from all three phase images to obtain

$$\varphi'_A = \varphi_A - \varphi_0,\ \varphi'_B = \varphi_B - \varphi_0, \text{ and } \varphi'_C = \varphi_C - \varphi_0 \qquad [3]$$

To find φ_1, a different angle θ is first calculated as a self-consistency check via

$$\theta = 2 \cdot \varphi'_A - \varphi'_C \qquad [4]$$

The basis for our phase-unwrapping method is that for each pixel, φ'_C should be two times φ'_A if there is no phase aliasing (ie, $\theta = 0$; see Table 1). If this is not the case (ie, $\theta \neq 0$), then phase aliasing must have occurred in the second in-phase image. In practice, because $|\theta|$ is either 2π or 0 ideally, a threshold of π was used to determine whether phase aliasing occurred. A lookup table (Table 2) was created to determine whether unwrapping was needed based on the value of $|\theta|$.

Rules (b) through (e) in Table 2 reveal those cases in which $|\theta|$ is nonzero and where φ'_C must have aliased. Under these circumstances, φ'_C can be unwrapped by adding or subtracting 2π. The following procedure was performed to determine whether 2π should be added or subtracted from φ'_C. First, a search algorithm was used to check each pixel line by line from left to right in the image and to find a pixel where $|\theta| > \pi$. This pixel was then used as a seed point in a 2D region-growing algorithm to determine all the connecting pixels in which $|\theta| > \pi$. Then, 2π was added to and subtracted from all pixels of this region in the φ'_C image to obtain two new phase images $\varphi'_C + 2\pi$ and $\varphi'_C - 2\pi$, respectively. Next, all the pixels were checked line by line from left to right in each of these two images and the phase differences between two adjacent neighboring pixels in the same image were calculated. If any of the phase differences were greater than a preset threshold, ie, 2π, a phase jump would be recorded. The phase image of $(\varphi'_C + 2\pi)$ and $(\varphi'_C - 2\pi)$ with the least number of phase jumps was taken to be the correct unwrapped phase value of the region and stored as a new image referred to as φ''_C. The above procedure was repeated throughout the rest of the θ image and φ''_C was updated for each region. Finally, the field inhomogeneity phase term was determined from:

$$\varphi_1 = \varphi'_C/2 \qquad [5]$$

Thus, within the limits of $-1.5 < \varphi_A \leq 1.5\pi$, φ_0 and φ_1 were free from aliasing.

From Table 2, it is readily seen that it was not possible to differentiate cases (f) and (g) from (a) based on θ only, ie, the aliasing is now irreversible and the true φ_1 can not be uniquely recovered.

Water and Fat Separation

Before processing the data for water and fat separation, the point of maximum magnitude in k space of the TE = 4.8 msec image was first detected and the k-space data were shifted so that the maximum was at the origin. This removes the phase shift caused by the asymmetric sampling. The phase of the echo center of the TE = 4.8 msec image was then subtracted from each point in k space. The same echo shift and phase subtraction were then applied to all three images.

A threshold was chosen in the magnitude image and the phase of all points with magnitude below the threshold was set to zero and not processed. After phase unwrapping, as described above, φ_0 and φ_1 were extracted and subtracted from the opposed-phase image. The phase value in the opposed-phase image should be either π (fatty tissue) or 0 (water tissue) in the ideal scenario. This phase was checked with a threshold of $\pi/2$ to determine whether the signal is water dominant ($<\pi/2$) or fat dominant ($\geq\pi/2$) on a pixel-by-pixel basis. Then, on a pixel-by-pixel basis, the sum of the magnitude of the average of the two in-phase images ($\bar{I}_{in}$) and that of the opposed-phase image (I_{opp}) was assigned to the dominant tissue, and the subtraction of the former from the latter was assigned to the other tissue. For example, if signal was water dominant, the water and fat components were calculated by

$$\rho_w = \frac{\bar{I}_{in} + I_{opp}}{2}, \qquad \rho_f = \frac{\bar{I}_{in} - I_{opp}}{2}. \qquad [6]$$

Volunteer Studies

Nine normal volunteers (four males, five females; age range, 15 to 35 years) were studied using the 2D and 3D gradient-echo sequences. All studies were performed on

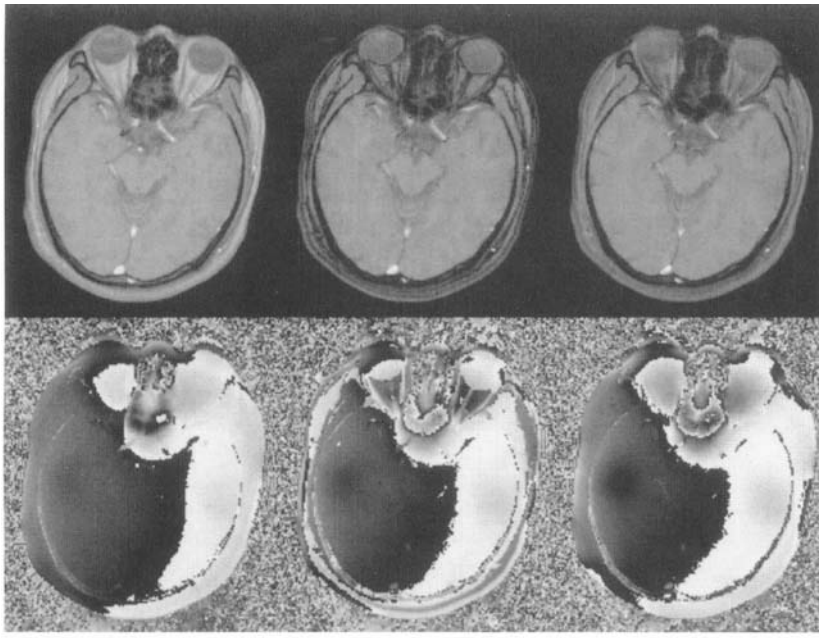

a.

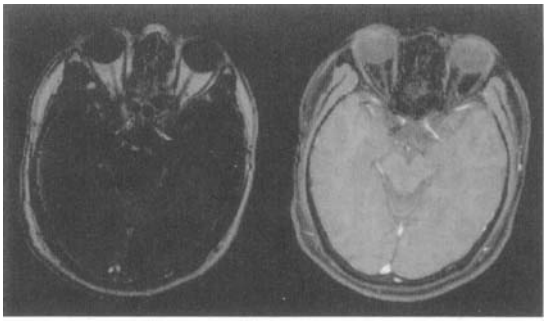

b.

Figure 2. **(a)** The original brain images of one slice in the orbit area. Top: three magnitude images; bottom: corresponding phase images. From left to right, the images correspond to water and fat being in phase, opposed phase, and in phase, respectively. All phase images presented here were without any phase filtering or echo shifting. Note the phase variation across the image, which could be removed by echo shifting. **(b)** The resultant fat (left) and water (right) images for the slice processed using the original images in **(a)**.

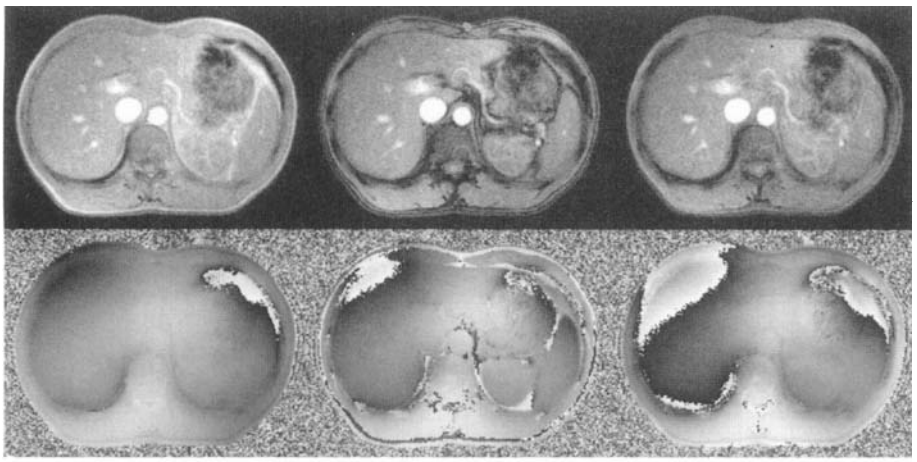

a.

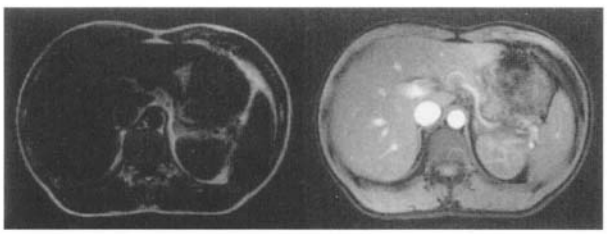

b.

Figure 3. **(a)** 2D breath-hold transverse images of a single slice in the abdomen. Top: three magnitude images; bottom: three phase images. From left to right, the images correspond to water and fat being in phase, opposed phase, and in phase, respectively. The phase images here were processed by echo shifting. **(b)** The resultant fat (left) and water (right) images processed from the original images in **(a)**.

a 1.5-T whole body imaging system (Vision, Siemens Medical Systems, Iselin, NJ). In three volunteers, brain images were obtained in the orbit area with both 2D and 3D sequences. A circularly polarized head coil was used. In four volunteers, knee images were obtained with 2D and 3D sequences using an extremity coil. The 3D sequence was run with flip angle = 30°, field of view (FOV) = 250 mm, matrix size = 256 × 256, slab thickness = 40 mm, and 64 partitions (effective slice thickness = .85 mm). For a given phase-encoding step, the TR affiliated with each of the three echoes was 35 msec, giving an effective TR of 105 msec. The echo center was located at the 70th point of a 256-point readout period to achieve velocity compensation for a TE of 4.8 msec. The 2D sequence was used in four volunteers for abdominal imaging to allow breath-hold scanning. The same imaging parameters as in the 3D sequence were used, except that the slice thickness was 4 mm and the FOV was 350 to 450 mm. With 192 phase-encoding steps, 2D scans could be acquired within 20 seconds.

Patient Study

A subject with a benign breast lesion was imaged using a breast coil with similar imaging parameters to those used in the volunteer studies, except the slab thickness was 128 mm with 64 partitions. Transverse 3D images

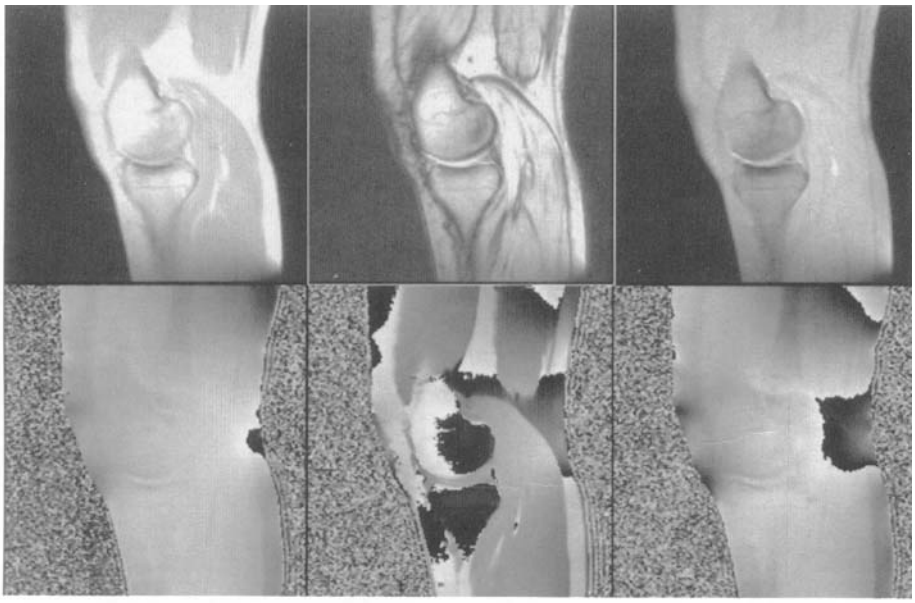

a.

b.

Figure 4. **(a)** A single partition image of the knee from a 3D data set. The three magnitude images are shown on the upper row, and the phase images are shown on the lower row. From left to right, the images correspond to water and fat being in phase, opposed phase, and in phase, respectively. The phase images shown here were processed by echo shifting. **(b)** 2D sagittal knee images: fat (upper left) and water (upper right). The time-invariant phase image φ_0 (left) and the linear phase map (proportional to the local magnetic field) φ_1 (right) are shown in the bottom row. Note that fat and water tissues have different φ_0 because of their different conductivities.

were collected both before and after contrast agent (gadolinium-diethylenetriamine pentaacetic acid [Gd-DTPA]) administration.

• RESULTS

An example of water and fat separation in the head is shown in Figure 2. In Figure 2a, three sets of original images are shown, with TE = 4.8 msec, 7.2 msec, and 9.6 msec, respectively. Note that in the opposed-phase magnitude image (second from the left on the top row), signal cancellation occurs, resulting in a lack of signal at water/fat boundaries. All three phase images show phase aliasing, and there is significant phase variation in the sinus area due to susceptibility changes at the boundary between air and tissue. The resultant fat and water images are shown in Figure 2b. Water and fat tissues were separated well around the orbit area. Optic nerve and fatty rings were well delineated. Some of the blood vessels appear in the fat image, which implies that the velocity compensation did not work perfectly.

In Figure 3, the water and fat separation in abdominal images are shown. These images were acquired with a 2D velocity-compensated sequence performed during a single 18-second breath-hold. Figure 3a is the original image set, with TE = 4.8 msec, 7.2 msec, and 9.6 msec from left to right, respectively. The resultant water and fat images are shown in Figure 3b. The separation appears successful throughout the image. From the fat image, it is readily seen that healthy human liver, kidney, and adrenal gland contain almost no fatty component. In clinical cases, the amount of fatty tissue in those organs may serve as a diagnostic criterion.

In Figure 4, 2D sagittal images of the knee are shown. In Figure 4a, three sets of original magnitude and phase images are shown, with TE = 4.8 msec, 7.2 msec, and 9.6 msec from left to right, respectively. The resultant φ_0,

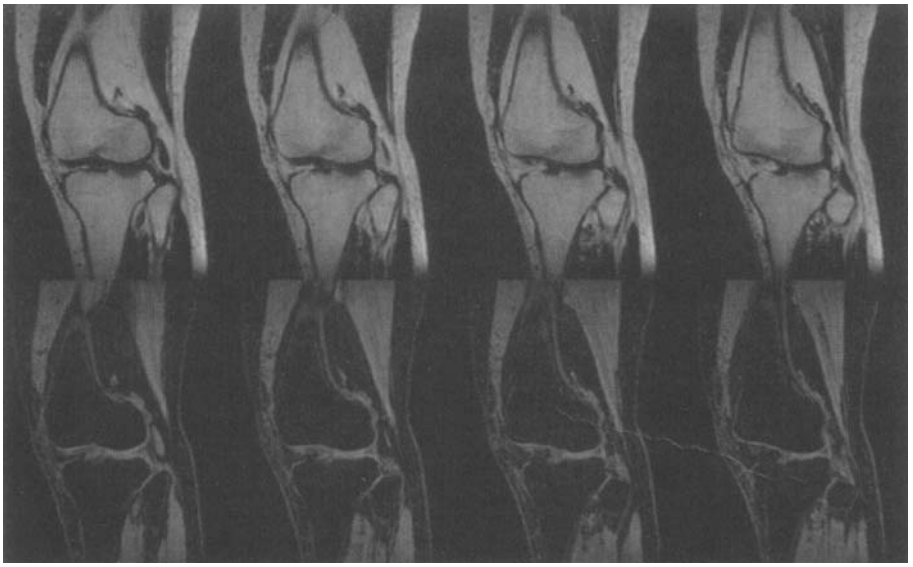

Figure 5. Four contiguous slices of sagittal knee images (top row: fat, bottom row: water) generated by processing a 3D data set. Each slice is .85 mm thick and the in-plane resolution in 1 × 1 mm².

φ_1, fat, and water images are shown in Figure 4b. Note the phase aliasing behind the knee in the original phase images; this is the area in which shimming does not work well. In the resultant water and fat images, this area is clear of artifact, demonstrating that the phase-unwrapping algorithm works well here. In Figure 5, 3D fat and water images of adjacent slices are shown. The in-plane resolution is 1 × 1 mm² Anatomical details about cartilage and blood vessels are clearly revealed.

In Figure 6, 3D transverse images of the breasts are shown after intravenous administration of .1 mmol/kg of contrast material (Magnevist; Berlex Laboratories, Wayne, NJ). The original in-phase and opposed-phase magnitude images are shown on the upper left and upper right portions of the figure, respectively. The fat (lower left) and water (lower right) images demonstrate that elimination of fat significantly improves water tissue visualization. In the water-only image, all fatty tissues were gone. The lesion (arrow), a fibroadenoma, shows marked contrast enhancement.

• DISCUSSION

Despite the diagnostic importance of quantifying water and fat signals, the Dixon method has not found wide clinical application. One of the reasons is the difficulty in unwrapping the phase reliably in the presence of local field inhomogeneities. Our phase-unwrapping method is based on a pixel-by-pixel comparison of the two in-phase images instead of just comparing the adjacent pixels in the same image. It makes use of the fact that the phase behavior of the two in-phase images in the three-point Dixon method is known and can be used to deduce the phase aliasing information by a simple consistency check of these two phases. Compared to other phase-unwrapping methods, our method is simple to implement and there is no requirement for user interaction. Furthermore, any errors that may occur in one part of the image will not propagate throughout the whole region, as they would with other segmentation methods. The fact that the data are interleaved makes the method robust in terms of motion or misregistration effects. Phase errors caused by noise could potentially cause errors in identifying phase aliasing and water and fat classification. Based on the criteria of phase consistency illustrated in Table 2, the minimal signal-to-noise ratio required for correctly detecting phase aliasing is approximately 1. Most of our images had a signal-to-noise ratio of greater than 10.

One of the important steps in removing phase errors caused by field inhomogeneities is the calculation of the time-invariant phase term φ_0. The φ_0 images demonstrate a tissue-dependent behavior, which was validated using a spin-echo imaging experiment in which the phase of the echo-centered image is exactly φ_0. In a typical φ_0 image, the phase shift between water and fat is less than 10°. The phase shifts between water and fat in the φ_0 image is mainly caused by the difference in tissue conductivity (24). These shifts were demonstrated in phantom studies (22). Nevertheless, in the presence of field inhomogeneities, the peak signal may not coincide with the center of k space in our method, which will cause global phase variations in the image. These phase variations were eliminated by shifting the peak signal to the center of k space. This will result in effective TEs only slightly different from those for water and fat to be in phase and opposed phase and will cause a tiny phase shift between water and fat in the calculated φ_0 image. A one-point shift in k space was often observed in our studies, which corresponds to a TE error of 20 μsec (with a 5.12-msec sampling time and 256 readout points) or a 2° shift between water and fat in the φ_0 image. This phase shift is present in all three images and is removed by subtracting φ_0 from the three phase images in our method. Therefore, this tissue-dependent φ_0 shift caused by the TE error will not affect the calculation of the true phase of the opposed-phase image and the determination of whether the tissue is water or fat dominant nor the actual calculation of water and fat components.

Our water and fat separation method calculates the true phase value in the opposed-phase image and uses it to determine whether the corresponding pixel is water or fat dominant. Magnitude images were used for the actual calculation of water and fat components. Errors occurring during field inhomogeneity correction may affect the determination of whether the tissue is water or fat dominant but will not affect the quantification of the water and fat signals.

In principle, the Dixon water-fat separation algorithm works only if water and fat spectra are δ functions. In practice, both water and fat spectra have a finite linewidth. The effect of this frequency spread is to cause a shorter effective T2* such as that seen in fat. The average

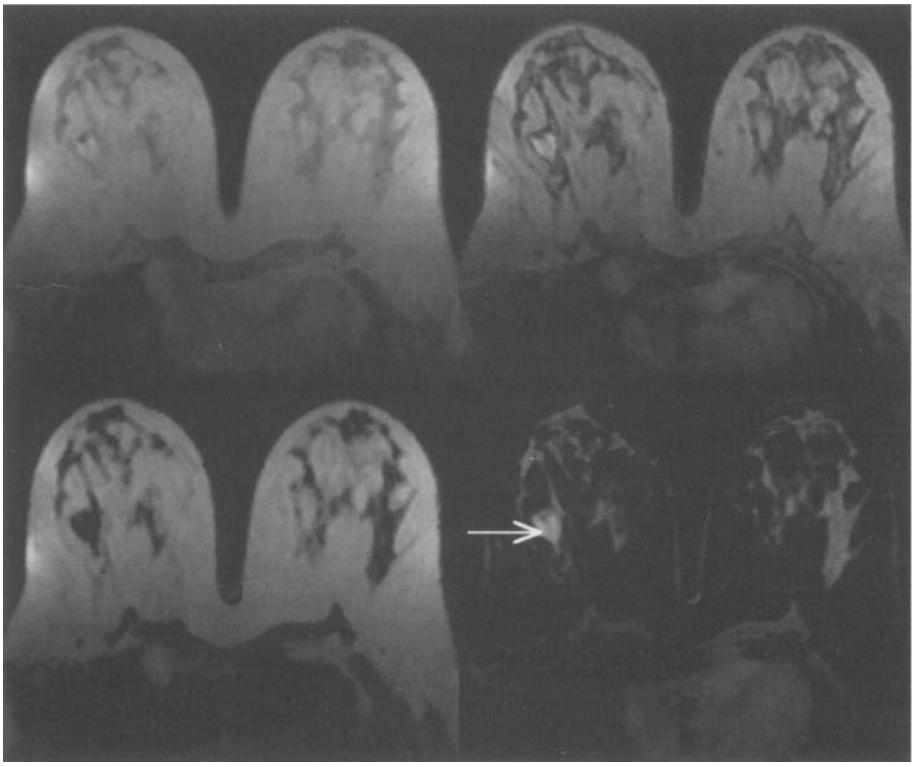

Figure 6. One slice of postcontrast 3D transverse breast images. Upper left: average of the two in-phase images; upper right: the opposed phase image. Lower left: the fat-only image; lower right: the water-only image. The lesion (arrow) in the right breast, a fibroadenoma, is the most enhanced structure after injection of the contrast agent.

of the two in-phase magnitude images was used as the in-phase image for the above calculation. Assuming the signal is a linear function of TE (TE << T2*), the averaged signal of TE = 4.8 msec and TE = 9.6 msec images should have the same weighting as the signal of the opposed-phase image (TE = 7.2 msec). A more general chemical shift imaging method has been proposed to deal with this effect (23).

Fast, pulsatile flow in major blood vessels can cause severe ghosting artifacts in the phase-encoding direction, which could contaminate the images for water-fat separation. The velocity compensation used in both readout and slice-select directions can significantly reduce this kind of artifact and improve image quality. In the body and leg images, the velocity compensation worked well; this is seen from the water images in which blood correctly appears. In the head, in which more rapid flow occurs in curved vessels, acceleration effects may be the cause of the remnant phase. In either case, the role of velocity compensation is very important.

As we showed earlier, the proposed phase-unwrapping method works when the phase shift in the first image is less than 270°, which means that the field inhomogeneity should be less than 5 ppm across the FOV. Although a larger phase error occurs less frequently today, it is still possible near the sinuses, lungs, and heart, where the susceptibility changes may induce a large field variation, or when a large FOV is used, such as in sagittal and coronal images. In these cases, a misclassification of the water and fat signals would occur. Fortunately, these peripheral areas often are not the regions of clinical interest.

Previous research (12,24) indicates that it is possible to acquire the three echoes after one excitation pulse by switching the polarity of the readout gradients. It is relatively easy to implement this at low field strength, for example, .35 T (12) or 1 T (24). It may be possible to implement this approach on a 1.5-T system with the high gradient capability of today's state of the art technology. The reasons why we did not follow that path are threefold. Although it reduces the imaging time, the phase artifacts induced by the different eddy currents of the fast switching gradient will make the phase information unreliable for the magnetic field correction. Furthermore, it is more difficult to compensate flow-induced phase. Finally, the image with a negative readout gradient will have a different geometric distortion from that with a positive gradient, which will cause phase mismatch and errors in water and fat separation.

In conclusion, we have developed a three-point Dixon method with a gradient-echo data acquisition and a pixel-based phase-unwrapping method to separate water and fat. This method requires no user interaction, allows for conventional short TR gradient-echo methods to be used throughout the body, and may find important clinical applications in whole body MRI.

References

1. Korobkin M, Lombardi TJ, Aisen AM, et al. Characterization of adrenal masses with chemical shift and gadolinium-enhanced MR imaging. Radiology 1995; 197:411–418.
2. Patrick JL, Haacke EM. Correction for geometric distortions in spin-echo images due to field inhomogeneities (abstract). Magn Reson Imaging 1985; 3:193.
3. Sun L, Aletras AH, Schmalbrock P, et al. Water and fat MR imaging with chemical shift selective 3D steady state methods. Magn Reson Med 1994; 31:359–364.
4. Poon CS, Szumowski J, Plews DB, Ashby P, Henkelman RM. Fat/water quantitation and differential relaxation time measurement using chemical shift imaging technique. Magn Reson Imaging 1989; 7:369–382.
5. Bydder GM, Young IR. MR imaging: clinical use of the inversion recovery sequence. J Comput Assist Tomogr 1985; 9:1084–1095.
6. Kaldoudi E, Williams SCR, Barker GJ, Tofts PS. A chemical shift selective inversion recovery sequence for fat-suppressed MRI: theory and experimental validation. Magn Reson Imaging 1993; 11:341–355.
7. Dixon WT. Simple proton spectroscopic imaging. Radiology 1984; 153:189–194.

8. Haacke EM, Patrick JL, Lenz GW, Parrish T. The separation of water and lipid components in the presence of field inhomogeneities. Magn Reson Med 1986; 1(2):123–154.
9. Glover GH, Schneider E. Three-point Dixon technique for true water/fat decomposition with B_0 inhomogeneity correction. Magn Reson Imaging 1991; 18:371–383.
10. Borrello JA, Chenevert TL, Meyer CR, Aisen AM, Glazer GM.mChemical shift-based true water and fat images: regional phase correction of modified spin-echo MR imaging. Radiology 1987; 164:531–537.
11. Hardy PA, Hinks RS, Tkach JA.mSeparation of fat and water in fast spin-echo MR imaging with the three-point Dixon technique. J Magn Reson Imaging 1995; 5:181–185.
12. Zhang W, Goldhaber DM, Kramer DM.mSeparation of water and fat MR images in a single scan at .35 T using "sandwich" echoes. J Magn Reson Imaging 1996; 6:909–917.
13. Szumowski J, Coshow W, Li F, Quinn SF. Phase unwrapping in the three-point Dixon method for fat suppression MR imaging. Radiology 1994; 192:555–561.
14. Yeung HN, Kormos DW. Separation of true fat and water images by correcting magnetic field inhomogeneity in situ. Radiology 1986; 159:783–786.
15. Simon JH, Szumowski J. Proton (fat/water) chemical shift imaging in medical magnetic resonance imaging. Invest Radiol 1992; 27:865–874.
16. Szumowski J, Coshow W, Li F, Coombs B, Quinn SF. Double-echo three-point-Dixon method for fat suppression MRI. Magn Reson Med 1995; 34:120–124.
17. Chan TW, Listerud J, Kressel HY. Combined chemical-shift and phase-selective imaging for fat suppression: theory and initial clinical experience. Radiology 1991; 181:41–47.
18. Keller PJ, Hunter WW, Schmalbrock P. Multisection fat-water imaging with chemical shift selective pre-saturation. Radiology 1987; 164:539–541.
19. Sepponen RE, Sipponen JT, Tanttu JI. A method for chemical shift imaging: demonstration of bone marrow involvement with proton chemical shift imaging. J Comput Assist Tomogr 1984; 8:585–587.
20. Hedley M, Rosenfeld D. A new two-dimensional phase unwrapping algorithm for MRI images. Magn Reson Med 1992; 24: 177–181.
21. Ching NH, Rosenfeld D, Braun M. Two-dimensional phase unwrapping using a minimum spanning tree algorithm. IEEE Trans Image Proc 1992; 1:355–365.
22. Haacke EM, Petropoulos LS, Nilgest EW, Wu DH. Extraction of conductivity and permittivity using magnetic resonance imaging. Phys Med Biol 1991; 36(6):723–734.
23. Wang Y, Haacke M, Yablonskiy D, Li D. Water and fat separation using chemical shifting imaging. In: Book of abstracts: International Society for Magnetic Resonance in Medicine 1996. New York: International Society for Magnetic Resonance in Medicine, 1996; 1636.
24. Hong X, Lian J, Kelly D, et al. Separation fat and water in MR images using triple-echo 3 point Dixon technique. In: Book of abstracts: International Society for Magnetic Resonance in Medicine 1995. Nice, France: International Society for Magnetic Resonance in Medicine, 1995; 646.